ELSEVIER

Ceramics International 33 (2007) 175–186

CERAMICS INTERNATIONAL

www.elsevier.com/locate/ceramint

Influence of gel-derived nanocrystalline spinel in a high alumina castable: Part 2

S. Mukhopadhyay *, P. Pal, B. Nag, P. Jana

College of Ceramic Technology, 73, A.C. Banerjee Lane, Kolkata 700010, India

Received 18 January 2005; received in revised form 15 May 2005; accepted 5 September 2005
Available online 20 December 2005

Abstract

An in situ spinel–alumina castable was prepared by incorporating 8.0 wt.% chemical grade pure magnesia fine in a high alumina-based low cement castable. Its porosity, density, spalling resistance and crushing strength were compared elaborately with the similar kind of refractory prepared with 8.0 wt.% of nano-dimensional spinel synthesized via sol–gel route. The microstructural aspects of both of them were carefully analysed, with special emphasis on the respective fired matrices by scanning electron microscopy (SEM) and the energy dispersive spectral (EDS) analysis. The co-precipitated spinel bonded specimen (CN) used in the previous work was also considered, particularly to estimate the rank of its slag corrosion resistance relative to the other two types. Infra red (IR) spectra and transmission electron microscope (TEM) micrographs of the selective additives with X-ray diffraction (XRD), hot modulus of rupture (HMOR), thermal shock behaviour of the selected castables were taken into consideration to evaluate the prospect of the gel-routed nanocrystalline additive.

Keywords: A. Sol–gel processes; B. Electron microscopy; C. Corrosion; D. Spinels; E. Refractories

1. Introduction

Nano-structured materials demonstrating unique features with impressive applications have received the primary focus of attention from the researchers belonging to a broad spectrum of disciplines [1]. Ceramic technologists, too, took profound interest to prepare and evaluate three-dimensionally modulated nanophase materials with precise properties. Refractory researchers recently started to engineer the quality of advanced castables by laying down nanosized materials in the respective fired matrix [2–6]. Very high surface energy and rapid diffusion paths usually make the fine nanoparticles far more reactive in the refractories, which frequently encounter the aggressive environment, particularly in the steel industries. As such, the strength, thermal shock and corrosion resistance of a refractory castable can be improved if one can favourably tailor the interaction of nanophases with the other matrix constituents.

Spinel-bonded high alumina castable is industrially synthesized from alumina and magnesia fines, which form in situ spinel ($MgAl_2O_4$) in a castable batch at high temperature [7–13]. The other commercial practice to prepare the same is to incorporate presintered spinel in the refractory batch. Such preformed spinels are obtained after a tedious and time-consuming procedure at excessively high sintering temperature [14] with inevitable ingress of pollution and contamination factors. No other method is frequently used to yield the spinel–alumina castable, although many novel routes have been suggested in literature for spinel preparation.

One such example is the sol–gel route, the tailorability of the products of which has been much appreciated in comparison with the traditionally manufactured materials. It avoids the important but inconvenient steps of the conventional processing, occurs readily with a wide variety of materials and can be conducted at near room temperature with a relatively small investment for equipments. Sol–gel method is also often utilized to prepare the nanomaterials from atomic/molecular precursors to gain most control over the submicroscopic aspect of the fired ensemble [15].

We had reported in detail the preparation of cost-competitive sol–gel derived (ultrapure and nanometric) spinel in laboratory [16–18]. In our previous work [5] a comparative study of the performance of a castable bonded with that sol–gel spinel had been done with alumina-rich commercially available presintered spinel. Another chemically prepared (co-precipitated)

* Corresponding author.
E-mail address: msunanda_cct@yahoo.co.in (S. Mukhopadhyay).

0272-8842/$32.00
doi:10.1016/j.ceramint.2005.09.009

micronized ultrapure spinel was also included in that investigation. In this work, chemical grade ultrapure magnesia fine has been used in the same high alumina-based castable batch, to imitate in part the industrial practice for fabricating in situ spinel–alumina castable. Its performance has been compared mainly with that of the sol–gel-based spinel and to some extent with the co-precipitated spinel powders [5,16]. The microstructural aspects of those fired castables were extensively studied to uphold the decisive influence of spinel nanoparticles in the refractory matrix.

2. Experimental

Light and pure chemical grade (LR) magnesia fine (Table 1) has been utilized in this work to prepare in situ spinel–alumina castable. Usually dead burnt (sintered or fused) magnesia is incorporated [19,20] in a high alumina castable batch to yield the same. As we compared the performance of MgO additive (code M) with that of ultrapure sol–gel (code G) and co-precipitated (code C) spinel additives, it was preferred to procure the pure chemical variety of magnesia fine (with negligible silica and alumina) available on the market. It resembles fairly the features of reactive caustic magnesia as used by other researchers for similar studies [11,21].

To maintain the consistency with our earlier work, an equal amount (8.0 wt.%) of this pure MgO fine has been incorporated into the same refractory batch (Table 2) as an in situ spinel-forming additive. This magnesia being too reactive, the water demand was too high for the castable batch coded as MN. The performance of this castable was compared primarily with that of sol–gel-based modified spinel (code GN), and with the same batch bonded by a co-precipitated spinel. The preparation of these pure nanosized (G) and micronized (C) spinel additives (Table 3) has been discussed and clarified in the earlier part of our investigation [5]. The flow property of the GN type has been found to be the best (>80.0%) among those three, as measured by conventional flow-value instrument [22]. The procedure for castable preparation included dry and wet mixing of the batch, both done thoroughly for 30 min to ensure the consistency of the mix. The mixed material was then cast in cubic (25.4 mm) moulds and gently tamped by hand within a certain time period. It should be noted that no extra vibrational facility was needed,

Table 1
Characteristics of light chemical grade magnesia powder

MgO (wt.%)	92.4
Crystal phase	Periclase
True-specific gravity	3.30
Average particle size (μm)	20.0
Surface area (m^2/gm)	10.3
SiO_2 (wt.%)	0.12
CaO (wt.%)	0.42
B_2O_3 (wt.%)	0.005
Al_2O_3 (wt.%)	0.04
Fe_2O_3 (wt.%)	0.03
Percent loss of ignition (including chloride, hydroxyl, carbonate and sulphate)	7.0 (approx.)

Table 2
High alumina-based castable batch containing spinel-forming additive in the matrix

Constituents	Content (wt.%)
Aggregate: white fused alumina (coarse, medium, fine)	75.0
Matrix (below 75 μm) Micronised alumina; two varieties in a definite proportion: (a) Reactive alumina, 7.7 μm (b) White tabular alumina, 11.3 μm	10.0
Microsilica: elkem grade (98% SiO_2, 0.88% L.O.I, 0.15 μm)	1.0
Refractory cement: Al_2O_3 74.2%, CaO 24.5%	6.0
Spinel additive [either as pure MgO fine, or as modified G or C powder (only one at a time)]	8.0
Total	100.0

as was the case throughout the course of this investigation [4–6,16–18]. Curing in humid condition (for 24 h), air drying (24 h) and oven-drying at 110 °C (for 3 days) were carefully done. This stringent schedule was followed finally by the heat treatment of samples (at a rate 5–8 °C/min) to 900, 1200, 1500 and 1600 °C, with a soaking of 2 h at each temperature. The rigidity of MN type castable at 110 °C was found to be very poor (explained later), while the handling strengths of the green GN and CN were satisfactory.

In the study of interaction of different spinel-forming materials with the fired matrix part of the castable, it was important to establish the nano-dimensional characteristics of the sol–gel additive as appeared in our last article [5]. As reported in literature [23–25], finer fractions below 75 μm may be treated as the matrix part of a castable batch. To understand the physicochemical changes taking place in the fired matrix of the spinel-bonded castable (Table 2), a simulated matrix composition of the spinel-free castable (Table 4) was prepared. The matrix compositions [23] of GN, MN and CN castables were formulated accordingly, by incorporating the respective contribution (at par with 8.0 wt.%) of each type spinel precursor. All of them were cast in identical conditions as

Table 3
Special features of chemically prepared (G and C type) modified spinel powders incorporated in the castable matrix

Characteristics	Sol–gel derived (G)	Co-precipitated (C)
Particle size (μm)	<75	<75
Crystalline phases fully appeared at (°C)	600	1000
Respective crystallite size (apparent)	18 nm	0.14 μm
Al_2O_3 (wt.%)	71.5	73.3
MgO (wt.%)	28.5	26.7
True-specific gravity	3.02	2.46

Table 4
Matrix composition of spinel-free castable

Constituents	Amount (wt.%)
Micronised alumina	58.80
High alumina/refractory cement	35.30
Micro silica	5.90
Total	100.0

described above and fired at 1500 °C/2 h. These specimens were chosen for electron microscope study (SEM) because that particular temperature was vital for both spalling and slag resistance tests, as discussed later. Also, a fine (−75 μm) basic slag (Table 5), collected from VSL (India) was gently rammed with the matrix of the GN type castable and fired at 1500 °C/2 h. This slag-affected GN matrix was subjected to an in depth SEM (with energy dispersive spectral (EDS)) study to understand the interplay of nanocrystalline spinel with the matrix and to improve the slag corrosion behaviour of the refractory.

The infra red (IR) spectral pattern of the supplied MgO fine was taken from an instrument 'Perkin-Elmer' by the KBr method. Bulk density (BD), apparent porosity (AP) and cold crushing strength (CCS) tests of castables were performed by standard methods [26]. An average of four samples was considered for all such tests. The HMOR study (1400 °C) of GN and MN castables was carried out by the same three-point bending method followed previously [5] with the bar (150 mm × 25.4 mm × 25.4 mm) specimens. The X-ray diffraction (XRD) phase analyses of the heat-treated castable samples were performed using a 'Philips Analytical' instrument with Ni-filtered Cu Kα radiation. For microstructural evaluation of the fired MN, GN and CN castables, scanning electron microscopy (SEM) (with energy dispersive spectroscopy) was conducted with the instruments JEOL JSM 5200 and Hitachi S-2300 models. The thermal shock resistance (spalling) test was carried out by the well-known water-quenching method (from 800 °C to cold water) as followed previously with the samples prefired at 1500 °C [4–6,16–18]. This value was reported in terms of percent residual strength (%RS) retained after 5 cycles of thermal shock. To distinguish between the slag resistance of three types of castables, the visual inspection of the cubes (both as a whole and cut section) was done in detail after the cubes were heat-treated with the supplied slag (Table 5). This test is similar to the conventional slag-cup test [27,28] with a simplified version done by the small cubic specimens prepared in laboratory. For this purpose, a cylindrical groove of the same dimension was made at the centre of the upper half of all those cubes in the green state after casting and preheated to 1200 °C for 2 h. The grooves were then filled up with that slag and fired at 1500 °C for 2 h. After normal cooling, the eroded samples were examined in terms of slag penetration and corrosion [10]. The slag corrosion of the GN castable sample was studied by SEM and EDS, as mentioned before.

Table 5
Composition of the converter slag (basic)

Constituents	Amount (wt.%)
CaO	47.6
SiO_2	15.0
MgO	10.6
FeO	20.5
Al_2O_3	1.3
MnO	2.0

To corroborate the sporadic nanosized features in the fired GN castable, as revealed in our previous communication, the microstructure of the same matrix was extensively studied in this work. For this reason, the TEM experiment of the finer fraction of calcined (1500 °C) powder of G additive was performed, to locate the retention of nanosized features of that spinel. The TEM instrument was the same Hitachi H-600 (bright field, 50 kV) model used in our last work.

3. Results and discussion

The IR studies of G and C powders have been reported in our last article [5]. Fig. 1 shows the IR spectral pattern of light chemical grade fine magnesia powder used in this work for preparing in situ spinel–alumina castable. The peak below 500 cm^{-1} can be ascribed due to the metal–oxygen linkage although a lot of other peaks are present; especially those nearby 3500 and 1400 cm^{-1}, which are possibly due to the presence of chloride, carbonate, hydroxyl and sulphate groups associated with the powder [29,30]. Table 1 shows that the true-specific gravity of this powder is less than that of the theoretical value of pure MgO. It may be therefore suggested that some unwanted ions are not completely removed [31] from this fine powder. The conventional practice before incorporating MgO fine in a refractory batch is to get it in the 'dead burnt' form to avoid the chances of hydration and cracking [32–34]. However, these materials prepared either from natural magnesite or sea-water magnesia, contain some amount of silica, alumina with lime and/or boric oxide [11,23,33]. These impurities (specially silica-bearing compounds) often have been reported to be beneficial for densification and hydration resistance [24,35].

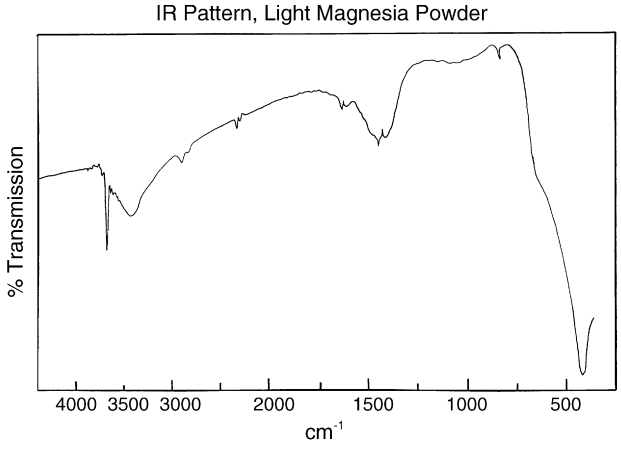

Fig. 1. Infra red (IR) spectral pattern of pure and light magnesia fine.

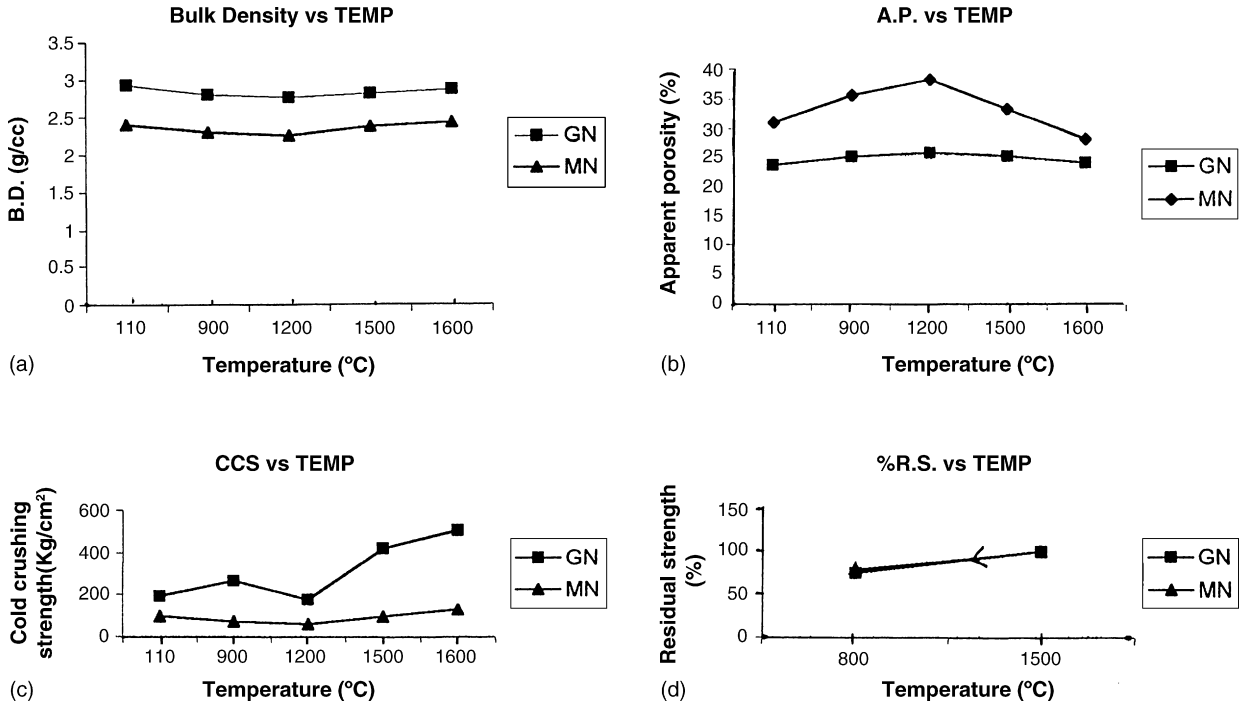

Fig. 2. Comparison of changes in properties GN and MN type castable in the range of (110–1600 °C): (a) BD; (b)AP; (c) CCS and (d) %RS (1500–800 °C).

We intended to compare the performance of a relatively pure (Table 1) grade MgO (calcined at relatively lower temperature), to that of pure sol–gel and co-precipitated spinel fines prepared in laboratory at 900 °C [5]. This magnesia was reasonable costwise and by and large similar to the caustic calcined magnesia. It is well reported [36,37] that this caustic MgO is very much reactive with small crystallite size and the dead burning turns it unreactive to avoid the hydration or shrinkage. In fact, the loss of ignition of it is usually high [36] because the breakdown temperature of carbonate etc. is higher than that of hydroxide. Some researchers often intended to use directly magnesium hydroxide [38] to avoid the hydration, however in this work, we wanted to study the consequence of adding reactive and pure MgO fine in the matrix. Although its loss of ignition (Table 1) and hydration resistance were the major shortfalls, its high surface area and purity were anticipated to enhance the slag corrosion resistance of the refractory as discussed below.

Fig. 2 shows a comparison between the changes in physical properties of the GN and MN castables (Table 2) with increasing temperature. As mentioned before, the performance of MN was very disappointing with very poor strength and enormous porosity. The addition of MgO fines has always been reported to be associated with severe hydration, heat evolution and dusting [39–41]. The poor BD, AP and CCS values at 110 °C have been echoed at high temperature, may be due to the consumption of excessive water by reactive MgO fines during casting [11]. The general pattern of both MN and GN castables resemble that of a typical low cement castable with an increase in porosity up to 900 °C, due to the gradual dissociation of cementitious hydrated (CAH_{10}, C_2AH_8, C_3AH_6 etc., where C = CaO, A = Al_2O_3, H = H_2O) compounds [42]. The increase in strength of GN within the intermediate temperature range, due

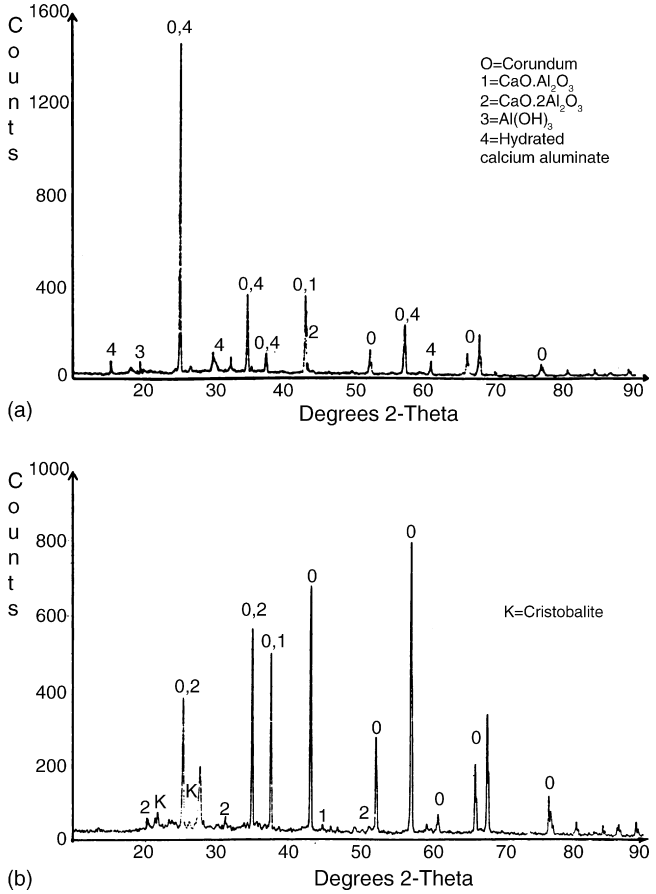

Fig. 3. XRD patterns of spinel free castable matrix heated at: (a) 110 °C for 2 h and (b) 1200 °C for 2 h.

chiefly to the nano-structured spinel additive, has been explained in our last article. Beyond 1000 °C, usually the strength of castable increases due to enhanced densification as observed in GN. The improvement in MN, however, was significantly low. As the SiO_2 and Al_2O_3 in the MgO fine (Table 1) used in castable matrix was negligibly small, it was difficult to achieve any advantage during sintering [24]. Moreover, as the solid-state reaction of MgO with Al_2O_3 is volume-expansive [9,43], it shattered the castables. The decomposition of brucite also created a series of cracks and pores in the MN refractory. Although these void spaces can be utilized to compensate the volume change during spinel formation, but no reasonable densification by diffusion during sintering is possible throughout the fired MN matrix. Consequently, its density had been found to be only slightly improved in the range of 1200–1600 °C during complete spinel formation. Only the spalling resistances (%RS) of GN and MN have been found to be comparable to each other. The thermal expansion mismatch between the Al_2O_3 fines present and the in situ spinel formed (in the matrix) might give rise to some microcracks [25], to increase the thermal shock resistance of MN by the crack-blunting mechanism. The volume expansion during spinelization may also generate such kind of flaws in the refractory.

The evolution of detrimental brucite in the MN type castable and its progressive disintegration become clear, when the XRD patterns of the spinel free castable matrix (Fig. 3) are compared with those of MgO bonded (MN) castables fired at higher temperatures (Fig. 4). Table 4, as mentioned before shows only the matrix composition of the castable without any spinel-forming material. Fuhrer et al. [25] considered the tabular alumina grains below 250 μm to be the matrix constituent of an in situ spinel–alumina castable composition. Ko considered the grains below 75 μm [23,24] to simulate the matrix part of a similar type castable formulation. We also followed this last case and consequently the white fused alumina (WFA) below 100 mesh BS sieve (i.e.150 μm) was included in the aggregate part of the batch along with the other coarse, medium and fine (−6 + 16, −16 + 30, −30 + 60 mesh) particles of WFA, the total being 75 wt.%. At 110 °C and 1200 °C, respectively the hydrated cementitious compounds (Fig. 3a) and the dehydrated calcium aluminate phases (Fig. 3b) are quite conspicuous [42] in the spinel-free matrix. The XRD pattern of the matrix part of MN type castable contains a reasonable amount of magnesium hydroxide from the very beginning (Fig. 4a). Beyond 900 °C this brucite converts to periclase phase (Fig. 4b) and possibly leads to a tremendous stress in the matrix. Only at 1200 °C (Fig. 4c) the periclase particles start reacting with alumina fines present in the matrix, to generate the spinel phase. The XRD pattern of 1600 °C fired sample (Fig. 4d) is similar to that already reported by Lee and co-workers [25]. The intensity of the peaks of spinels increases remarkably with a noticeable decrease of corundum and hibonite ($CaO{\cdot}6Al_2O_3$) phases. Such a tremendous increase

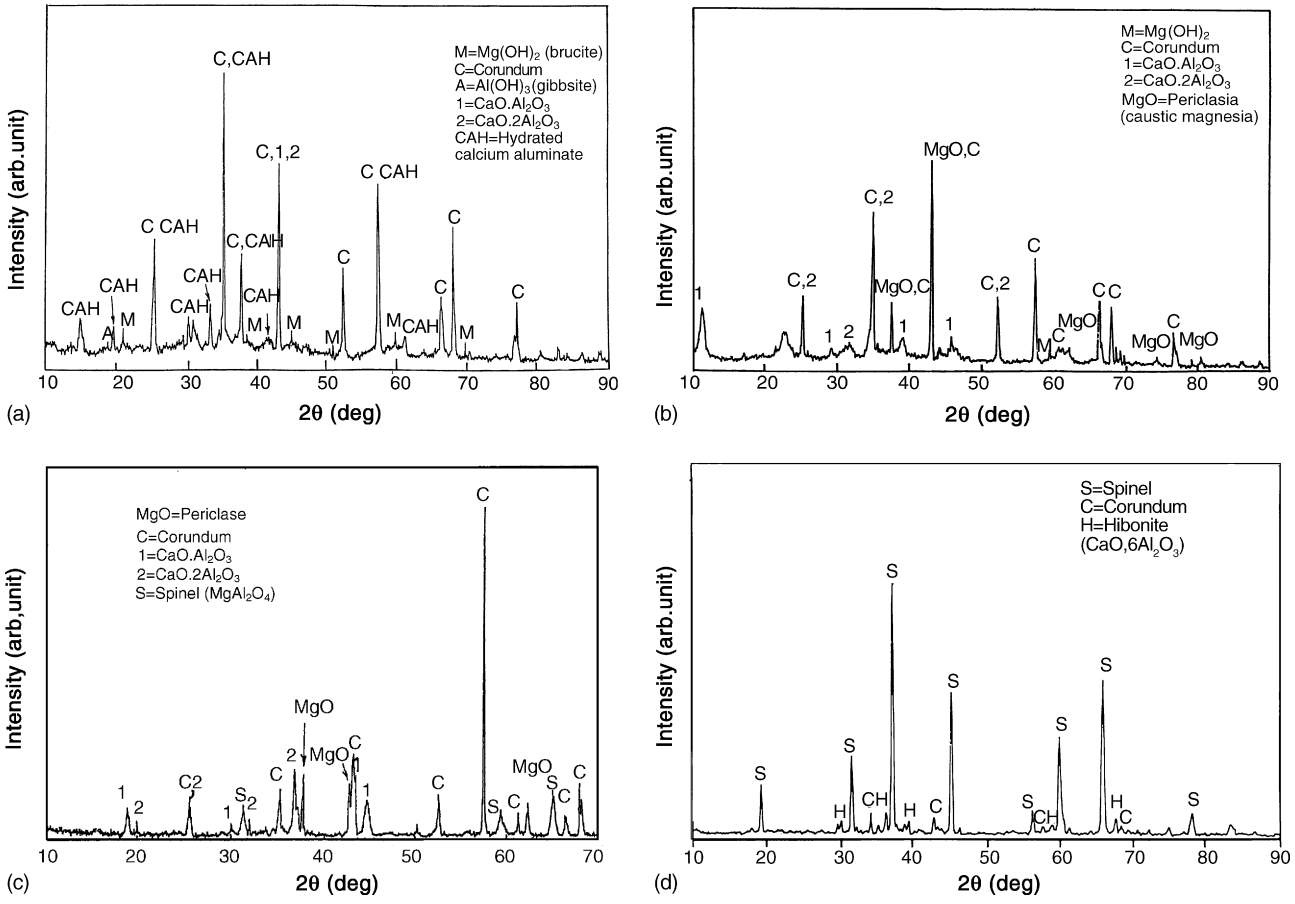

Fig. 4. XRD patterns of MN type castable heated at: (a) 110 °C for 2 h; (b) 900 °C for 2 h; (c) 1200 °C for 2 h and (d) 1600 °C for 2 h.

in the quantity of spinel solid solution might have a positive effect on the slag corrosion resistance of the MN castable. At the same time, the decreased proportion of alumina and hibonite in MN must adversely affect the strength of the castable. It has been reported [44] that the matrix-advantage-system in such a castable can be incurred only if the linkage of spinel–hibonite–corundum can be designed properly. The same linkage can be developed appreciably in the GN type castable [6] with nanocrystalline sol–gel-derived spinel, to achieve reasonable CCS (Fig. 2) and HMOR value (120 kg/cm^2). On the contrary, the poor connectivity among the spinel, corundum and hibonite grains in the MN type leads to a very low HMOR value (54 kg/cm^2) as also supported by other researchers [45]. This observation becomes more obvious when the microstructures of the respective castables are observed.

Fig. 5 shows the microstructural evolution of GN castable at elevated temperature. The net-like morphology, as observed at 1600 °C in Fig. 5(a) is very much desirable in spinel–alumina castable. This kind of structure, enriched with the CaO–MgO–Al_2O_3–SiO_2 (CMAS) phase has already been reported to exert some beneficial role towards the castable performance [25,46]. It is to some extent refractory [47,48] and efficiently holds the corundum and hibonite grains with the spinel phases present in the matrix. The EDS pattern (in Fig. 5a) confirms the presence of well-developed CMAS phase in GN castable. The presence of viscous CMAS phase might also assist to hold the crack-faces

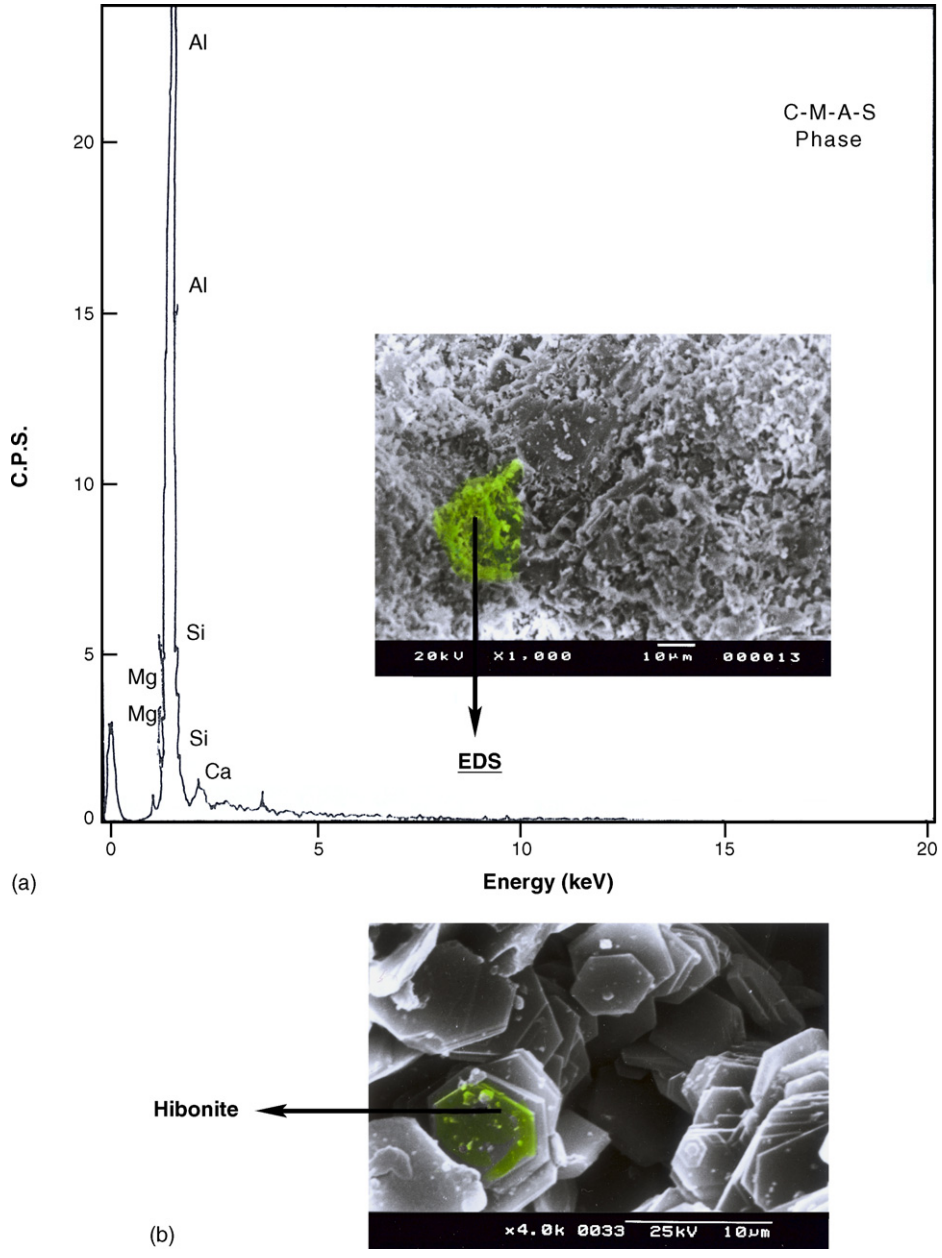

Fig. 5. (a) SEM micrograph of GN castable fired at 1600 °C for2 h, with the EDS pattern of a selected region; (b) SEM micrograph of fired (1600 °C) GN castable with hexagonal crystals in the matrix; (c) SEM micrograph of the fired matrix (1500 °C) of GN castable with nanocrystalline spinel in the matrix and (d) TEM of G type fine spinel powder calcined at 1500 °C for 2 h.

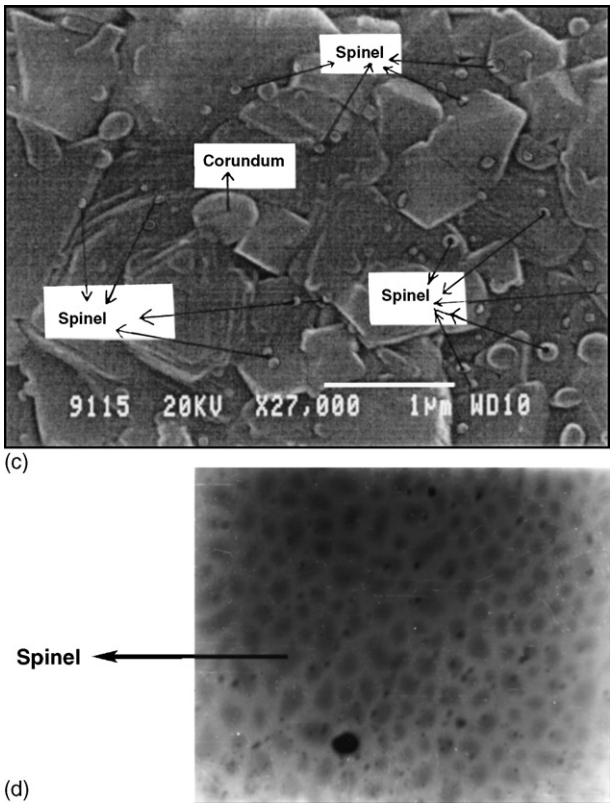

Fig. 5. (*Continued*).

together during thermal shock to enhance the maximum work of fracture of the castable-matrix [49]. Fig. 5(b) clearly shows plenty of card-like hexagonal hibonite phases in the fired castable. It may be suggested that the matrix-advantage-system [44] in this castable has been developed due to the high degree of three-dimensional connectivity of hibonite and corundum grains with the reactive nanocrystallites of spinel additive. Fig. 5(c) shows the fired (1500 °C) matrix of GN refractory which again confirms the presence of well-dispersed nanophase spinel particles throughout the matrix. These inter- and intra-granularly distributed spinel fines must have some influence to improve the slag corrosion and thermal shock properties of GN castable. Apart from the contribution of the distributed micropores created in the fired castable [50,51], the sporadic nanosized spinel crystallites might also hinder the extension of cracks in the castable matrix [52]. Such kind of flaw-tolerant crack-bridging behaviour of the ceramic matrix can definitely improve the spalling resistance [53] of the GN castable. This particular matrix having a substantial amount of reactive nanosized spinel phases would also help to efficiently engulf the unwanted ions from slag as clarified later. The TEM micrograph of the gel-derived (G type) modified additive displayed before [5], clearly indicated the presence of spinel nanoparticles. The lower tendency of such particles to get aggregated, has been further substantiated by the Fig. 5(d), whose scale is almost equal to that of Fig. 5(c). This TEM figure firmly infers that the powder preserves its nanodimension, even after calcination at 1500 °C. Such kind of retention of nanofineness at higher temperature is another benefit of the sol–gel route exploited here. Those reactive particles, as outlined later, may give an additional advantage towards the slag corrosion behaviour of the GN castable, by maintaining the nanostructure of the respective matrix.

Fig. 6(a) shows the all-pervasive spinel in the matrix of the MN type castable, the grains being larger than in the GN type. Here also the net-like morphology and CMAS phase have been observed (Fig. 6b) but the intensity of the latter is much less than in GN as revealed from the EDS pattern. As the formation of abnormal grains of spinel in MN matrix is extensive above 1500 °C, it might be possible that the CMAS phase has not been grown properly in the respective castable. Kobayashi et al. [7] reported an optimum composition of Al_2O_3–MgO castable with 7.5 wt.% MgO and 0.5 wt.% microsilica. In our composition, the amount of microsilica was 1.0 wt.% (Table 2) from the very beginning, to carry out a uniform comparison with all the varieties of castables. It has been found that some amount of microsilica is necessary for the in situ spinel–alumina castable to reduce the explosive spalling [11,38] and to render the flexibility of installation. Some of the relevant reports suggest that an optimum ratio of MgO/SiO_2 is required to ensure appreciable spinel formation [25]. The spinel formation in the MN castable might also have been accelerated due to microsilica and consequently the amount of CMAS has been reduced. The enormous amount of spinel present at elevated temperature has already been corroborated from the respective XRD pattern (Fig. 4b) with a concomitant decrease of hibonite and corundum phases. Theoretically, 8.0 wt.% MgO present in MN castable should yield almost 28.4 wt.% spinel [23], if the reaction is complete. This reaction might have decreased the alumina content in the matrix with an inevitable weakening of the spinel–hibonite–corundum linkage. As a result, the adverse effects, e.g. high porosity (around 35%) and low CCS already created due to the decomposition of brucite, were very much difficult to compensate later, by sintering alone. Fig. 6(c) shows the micrograph of the fired matrix of the CN castable (Table 2). The CN has no trace of spinel nanocrystallites and resembles the MN matrix, with relatively large sized grains of spinel amidst the corundum and hibonite phases. In our earlier communication, the poor performance and microstructure of this material have been discussed, along with the important features of the C additive.

Fig. 7 represents the visual observation of the corrosion effect in the GN, MN and CN castables simulated by heating in a corrosive slag (Table 5). Those photographs advocate that the performance of MN was the best among them in terms of slag penetration and corrosion [10,24]. The slag resistance of the CN type castable (i.e. the distorted cube) was low, while that of GN could be of interest as indicated in our last paper, and further explained here. The conventional in situ spinel–alumina castables (similar to MN) have established a consistently successful record of slag resistance [10,11,20,23]. As opined by Ko [24], the contact angle criterion (related to solid–liquid interfacial energy) and the viscosity parameter of slag (enhanced by MgO precipitation) strongly assist the MN castable to exhibit such good performance. Moreover the extensive in situ spinellisation, might also influence positively the slag resistance property. In spite of this, it is evident from

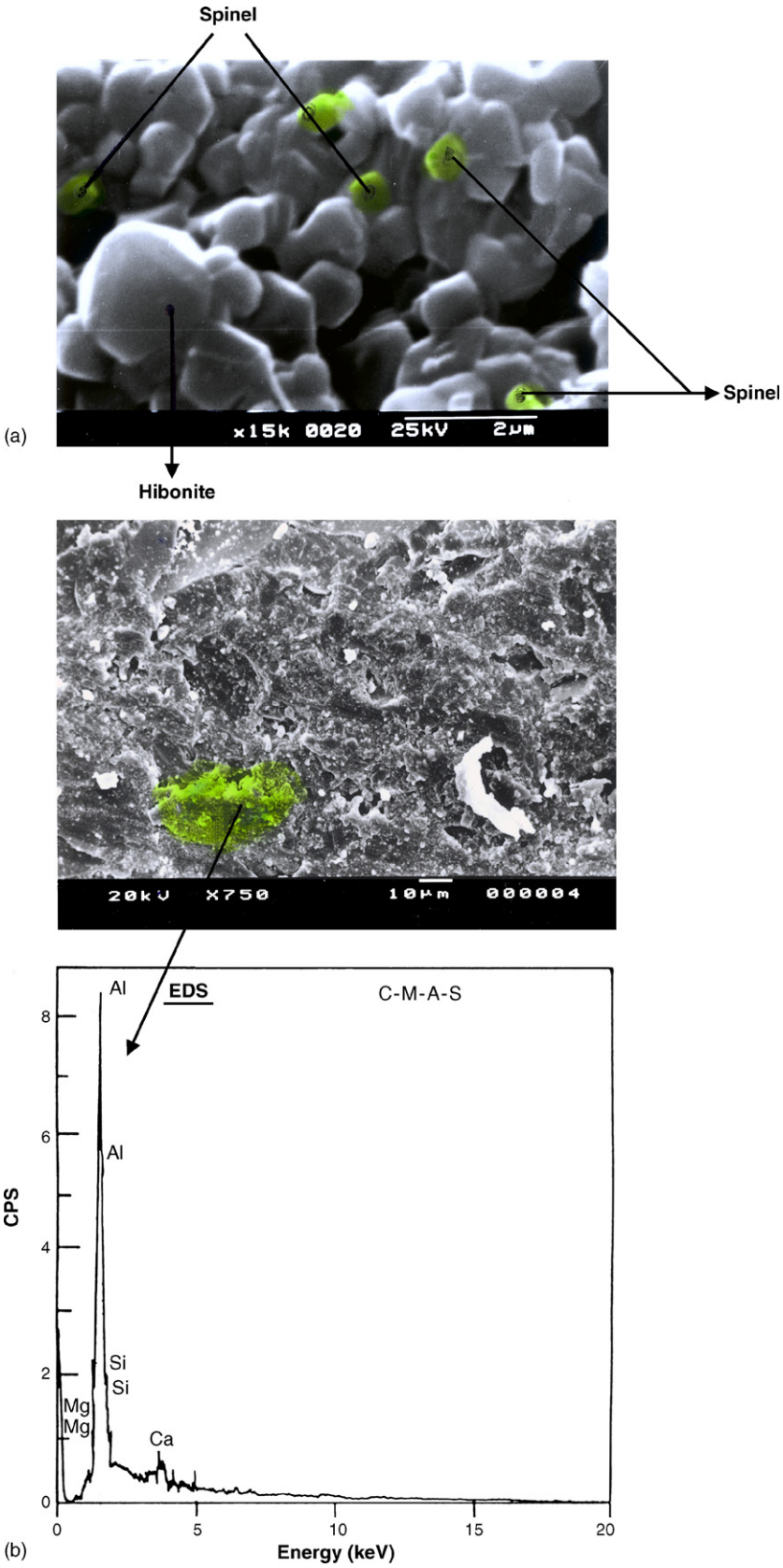

Fig. 6. (a) SEM micrograph of the fired matrix (1500 °C) part of MN castable; (b) SEM micrograph of MN castable fired at 1600 °C for 2 h with the EDS pattern of a selected region and (c) SEM micrograph of the fired matrix (1500 °C) of CN castable.

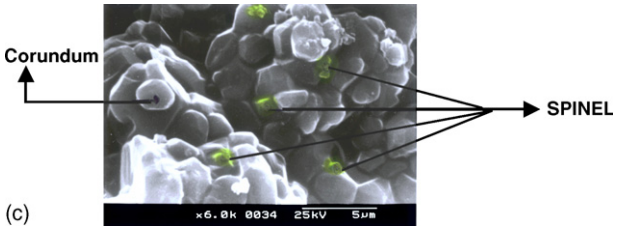

Fig. 6. (*Continued*).

Fig. 7(b) that the penetration resistance of MN (in downward direction) was not as high as the corrosion resistance in lateral direction. Recently Sasaki et al. [10] held a similar view by a systematic comparison between the corrosion and penetration index-values changing with the amount of MgO fine present in the batch. That article assigned an optimum amount of magnesia, typically around 8.0 wt.%, above which the slag penetration starts to deepen while the slag-wetting behaviour in lateral direction is less extensive. The large permeable pores already generated in the MN castable might worsen the penetration resistance when the amount of MgO is raised beyond this 8.0% limit. Therefore, not only the amount of spinel particle is important for slag corrosion resistance property, but also the textural changes occurring in castable due to the spinel-forming additive. However, both the Fig. 7(a) and (b) suggest that the penetration and corrosion resistances are optimally controlled in the GN castable and this may lead to a practical importance of the respective sol–gel powder.

The uniformity of nanoscaled spinels with exceedingly high surface area (Fig. 5c and d), possibly render a perfect matrix-advantage-system [6,44] by sticking strongly to the surrounding corundum and hibonite grains. This has certainly increased the contact area between the grains to promote the BD and CCS (Fig. 2) of GN castable at elevated temperatures. Apart from improving the HMOR value by forming this network of spinel–hibonite–corundum, an enormous interfacial area generated by these nanometric spinels also assisted the slag corrosion property. Actually such spinel nanoparticles are associated with some residual hydroxyl groups, as discussed in our previous paper [5]. During heat-treatment they create some fine pores nearby, after the expulsion of such (OH) groups. When these micropores are distributed in a refractory, greater pressure is needed by the corrosive media to penetrate them [54], because such pores are rapidly covered by that fluid. Thereafter, the relicts of these nano-structured additives remain close to the hibonite and corundum grains to disappear gradually by the

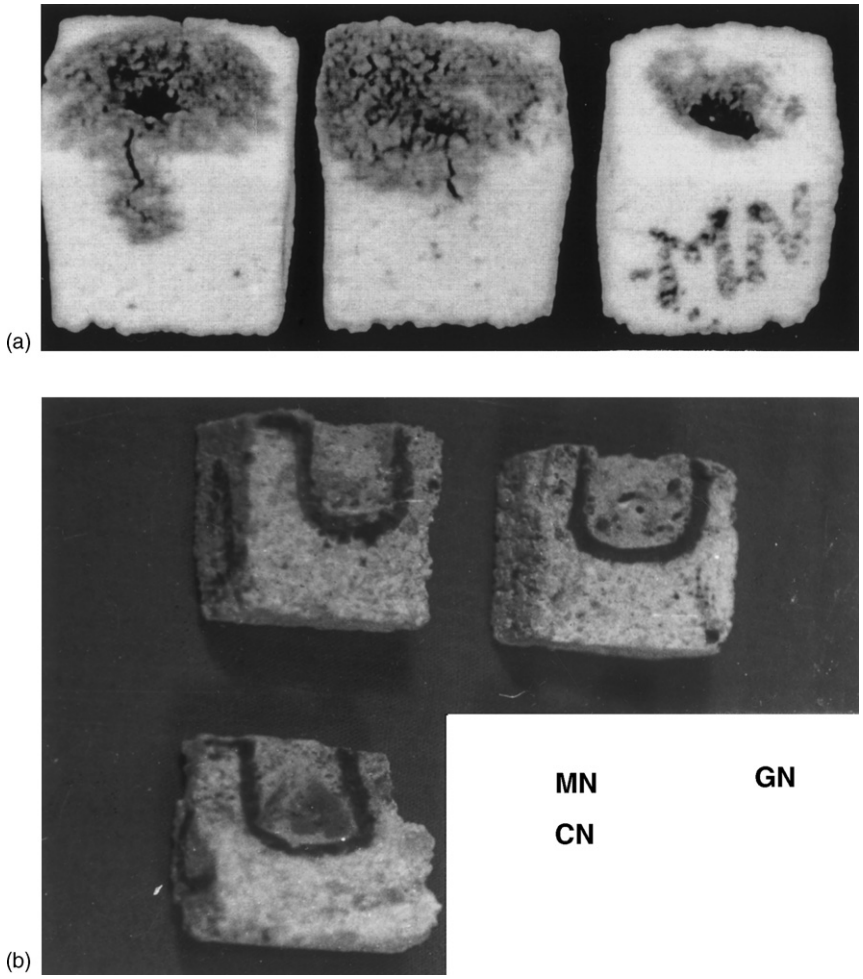

Fig. 7. Photographs of slag corroded castables: (a) full cubes (from left—CN, GN, MN types); (b) cut section of the cubes and (c) SEM micrograph of the slag corroded matrix (1500 °C) of GN castable with the EDS pattern of a selected region.

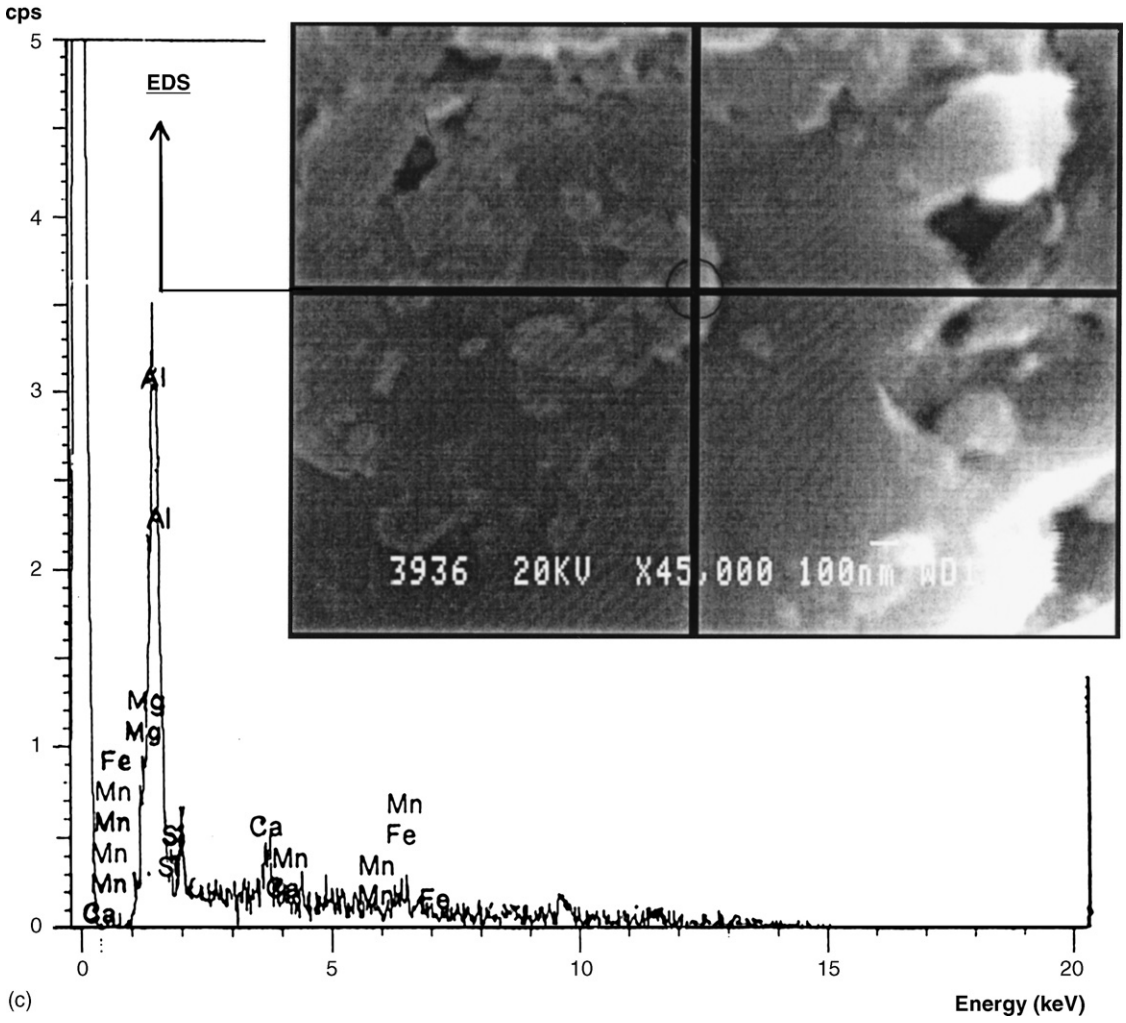

Fig. 7. (*Continued*).

reaction with aggressive slag. It is obvious that the layer surface of the nanophase grains differs in the coordination and local site symmetry from the bulk [55] and is associated with more energy to absorb readily the ions from the contact zone. While considering the corrosion of a refractory by a glass [56], nature of the refractory surface and its microstructure are immensely important. It is also known that it is difficult for a glass to penetrate between the unlike grains than between the like grains. Consequently, a large dihedral angle (with less wetting) associated with the small nanosized grains attached to the corundum and CA_6 phases, effectively improve the resistance of the GN castable to slag attack. The spinel phase is always desirable to form a barrier coating [57] at the slag refractory interface. When the sol–gel routed ultra fine remnant spinels are distributed homogeneously in the matrix, it obviously becomes difficult for the slag to invade the refractory. Fig. 7(c) once more strongly supports this nano-dimensional characteristics of the G type spinel additive. It has been well documented [58] that, among the several parameters involved in the corrosion of a refractory, a dominant role is played by the viscosity of the corroding medium [59]. $MgAl_2O_4$ spinel in castable is known to engulf the Mn^{2+}, Fe^{2+} ions from the slag [60] to control its fluidity. The crossover point in the SEM figure (Fig. 7c) of the slag-corroded GN matrix confirms the presence of those unwanted ions in the complex spinel solid solution at the vicinity of a glassy environment of C-A-S phase. Such kind of entrapment of Mn^{2+}, Fe^{2+} ions from slag might have been made possible by the reactive nanosized spinels present throughout the matrix. As a result the viscosity of the rest part of glass (silica rich) is enhanced and it becomes very difficult for them to disrupt the less permeable castable matrix [11,24]. This kind of nanocrystalline structure is now also known to be useful in retarding the corrosion-assisted cracking, by minimising the stress intensity at the crack-tip [61]. The SEM figure (Fig. 7c) also shows the micropores present in the matrix, which were beneficial [5] for the spalling resistance of GN castable.

4. Conclusions

From the laboratory scale investigation, it can be postulated that the gel-routed pure and nano-structured spinel fines perform much better in castables than the chemical grade pure fine magnesia additive. The latter shows good slag corrosion and comparable spalling resistances, although a severe

hydration and disintegration of reactive magnesia powder present in castable matrix put a serious limitation towards its practical application. Another newer class of spinel–alumina castables, derived by 8.0 wt.% of co-precipitated pure spinel fine, was not very impressive. The sol–gel derived spinel-bonded castable matrix showed commendable performance, especially, thermal shock and slag resistance behaviour in the corrosive environment of the secondary refining of steel. Consequently, the preparation of cost-effective nanometric spinel powder, if made suitable for commercial scale, should be in the attention of the refractory makers.

References

[1] P. Janeway, Nanotechnology—its more than size, Am. Ceram. Soc. Bull. 82 (4) (2003) 31–38.

[2] S. Tamura, T. Ochiai, T. Kanai, H. Nakamura, Nanotech refractories-1: the development of nanostructural matrix, in: Proceeding of UNITECR-03, 19–22nd October, Osaka, Japan, 2003, pp. 517–520.

[3] Y.E. Pivinskii, P.V. Dyakin, Y.Y. Pivinskii, S.V. Vikhman, Nanoparticles and their effective use in the technology of highly concentrated binding suspensions (HCBS) and refractory castables: part-2, Refract. Ind. Ceram. 44 (5) (2003) 314–318.

[4] S. Mukhopadhayay, P.K. DasPoddar, Role of nanocrystalline spinel additive on the properties of low cement castable refractories, in: Proceedings of International conference on Nanomaterials: Synthesis, Characterisation and Application, McGrawHill publication, 4–6 November, Kolkata, India, 2004), pp. 350–360.

[5] S. Ghosh, S. Sen, T. Maiti, S. Mukhopadhyay, Influence of gel-derived nanocrystalline spinel in a high alumina castable: part-1, Ceram. Int. 31 (2) (2005) 333–347.

[6] S. Mukhopadhyay, P.K. DasPoddar, Modified in situ spinel–alumina castables, Ceram. Silikaty 48 (3) (2004) 100–109.

[7] M. Kobayashi, K. Kataoka, Y. Sakamoto, I. Kifune, Use of alumina–magnesia castables in steel ladle side wall, Taikabutsu Overseas 17 (3) (1997) 39–44.

[8] J. Mori, S. Tanaka, Y. Twilani, Development of Al_2O_3–MgO castables for steel ladles, in: Proceedings UNITECR-95, vol. 3, pp. 171–78, Kyoto, Japan.

[9] M. Rigaud, C. Xing, V. Kovac, Volume stability of spinel-bonded magnesia castables, Euroceramics V, Key Eng. Mater. 132–136 (1997) 1818–1820.

[10] H. Sasaki, R. Nakamur, T. Kaneshige, M. Namba, Development of spinel–magnesia castable for steel ladles, in: Proceedings of UNITECR-2003, Osaka, Japan, pp. 666–669.

[11] A. Molin, J. Molin, J. Podworny, T. Wala, Study on slag resistance of in situ spinel-based ULC castable refractories, in: Proceedings of UNITECR, Osaka, 2003, pp. 576–579.

[12] P. Nandi, A. Garg, R.K. Singh, B.D. Chattaraj, Influence of silica and magnesia on in situ spinel formation in alumina–magnesia castable, Br. Ceram. Trans. 103 (3) (2004) 134–138.

[13] P. Nandi, A. Garg, R.K. Singh, B.D. Chattaraj, Effects of cement and magnesia fines on in situ spinel formation in alumina–magnesia castable, Adv. Appl. Ceram. 104 (2) (2005) 83–88.

[14] C.-J. Ting, H.-Y. Lu, Deterioration in the final stage sintering of magnesium aluminate spinel, J. Am. Ceram. Soc. 83 (7) (2000) 1592–1598.

[15] A.N. Goldstein, Hand book of nanophase material, Marcel Dekkn Inc, New York, 1997, p. 44.

[16] S. Mukhopadhyay, S. Sen, T. Maiti, M. Mukherjee, R.N. Nandy, B.K. Sinhamahapatra, In situ spinel-bonded refractory castable in relation to coprcipitation and sol–gel derived spinel-forming agents, Ceram. Int. 29 (8) (2003) 857–868.

[17] S. Mukhopadhyay, P.K. DasPoddar, Effect of preformed and in situ spinels on microstucture and properties of a low cement castable, Ceram. Int. 30 (3) (2004) 369–380.

[18] S. Mukhopadhyay, P.K. DasPoddar, G. Banerjee, Proceedings of UNITECR-2003, Influence of Prereacted and Self-reacting Spinels on the Characteristics of High Alumina Castable, pp. 158–161.

[19] T. Okada, J. Yagi, A. Hayashi, T. Kawakami, K. Yasua, S. Kuroki, Improvement of castable refractories for top bubbling lances, Taikabatsu Overseas 18 (1) (1998) 33–37.

[20] T.F. Veeza, T. Richtr, R.A. Lamdaer, Slag corrosion mechanisms of cement free Al_2O_3–MgO castable, in: Proceedings of UNITECR-1997, vol. 1, New Orleans, pp. 23–32.

[21] D. DasPoddar, S. Mukhopadhayay, Spinel-bonded basic castable in relation to spinel-forming agent, Interceram 51 (4) (2002) 282–287.

[22] ASTM C-230 procedure.

[23] Y.C. Ko, Influence of the characteristics of spinels on the slag resistance of Al_2O_3–MgO and Al_2O_3–spinel castables, J. Am. Ceram. Soc. 83 (9) (2000) 2333–2335.

[24] Y.C. Ko, Role of spinel composition in the slag resistance of Al_2O_3–spinel and Al_2O_3–MgO castables, Ceram. Int. 28 (7) (2002) 805–810.

[25] M. Fuhrer, A. Hey, W.E. Lee, Microstructural evolution in self-forming spinel/calcium bonded castable refractories, J. Eur. Ceram. Soc. 18 (1998) 813–820.

[26] ASTM C 20-00 and C 133-94.

[27] C.A. Schacht (Ed.), Refractories Handbook; D.A. Brosnan, Corrosion of Refractories, Marcel Dekker Inc., New York, 2004, p. 75.

[28] R.E. Fisher (Ed.), Ceramic Transactions, vol. 4, Advances in Refractories Technology, A.C.D. Chakladar et al., Development of slag-resistant refractories, Am. Ceram. Soc., Ohio, 1989, pp.489–505.

[29] L.-C. Dufour et al. (Ed.), Surface and Interfaces of Ceramic Materials, J.J. Hoagland et al., A Vibrational Study of Tetracyanoethylene Adsorbed on MgO, NATO ASI series (Applied Sci), vol. 173, Kluwer Academic Publishers, USA, 1989, pp. 155–163.

[30] B. Smith, Infrared Spectral Interpretation: A Systematic Approach, CRC Press, LLC, USA, 1999.

[31] C.E. Scott, J.S. Reed, Analysis of Cl ions laundered from submicron zirconia powders, Am. Ceram. Soc. Bull. 57 (8) (1978) 741–743.

[32] W. Ryan, Properties of Ceramic Raw Materials, 2nd ed., Pergamon Press, New York, 1978, pp. 91–93.

[33] W.E. Worrall, Clays and Ceramic Raw Materials, Applied Science Pub. Ltd., London, 1975, pp.179–181.

[34] W.D. Kingery, Structure and properties of MgO and Al_2O_3 ceramics, advances in ceramics, vol. 10, O.J. Wittemore et al. (Ed.), Model of interaction between magnesia with water, Am. Ceram. Soc., Ohio, 1984, 592–600.

[35] A. Kamyasu, S.-I. Yamamoto, T. Watanabe, A. Kanyasu, MgO raw materials with improved hydration resistance, Taikabutsu Overseas 16 (2) (1996) 26–30.

[36] J.H. Chesters, Refractories: Production and Properties, The Institute of Materials, pp. 130–143, 199.

[37] C.A. Schacht (Ed.), Magnesia Refractories; R.A. Landy, Corrosion of Refractories, Marcel Dekker Inc., New York, 2004, pp. 109–150.

[38] P. Nandi, A. Grag, B.D. Chattaraj, M.S. Mukhopadhyay, Effect of silica and temperature on spinel-based high alumina castables, Am. Ceram. Soc. Bull. 79 (12) (2000) 65–69.

[39] K.G. Aghari, J.H. Sharp, W.E. Lee, Hydration of refractory oxides in castable bond system-1; alumina, magnesia and alumina–magnesia mixtures, J. Eur. Ceram. Soc. 22 (4) (2002) 495–503.

[40] S. Zhang, S. Hashimoto, W.E. Lee, Effects of magnesia and calcium aluminate cement on the hydration of Al powder in castables matrix, in: Proceedings of UNITECR-2003, pp. 643–46, Osaka, Japan.

[41] P. Lauzon, J. Rigby, C. Oprea, T. Troczynski, G. Oprea, Hydration studies on magnesia-containing refractories, in: Proceedings of UNITECR-2003, pp. 54–57, Osaka.

[42] N. Schmitt, J-F. Hernandez, V. Lamour, Y. Berthaud, P. Meunier, J. Poirier, Coupling between kinetics of dehydration, physical and mechanical behaviour for high alumina castable, Cement Concrete Res. 30 (10) (2000) 1597–1607.

[43] K.H. Hwang, K.D. Oh, R.C. Bradt, In situ spinel bond formation (expansion/contraction) during firing, in: Proceedings of UNITECR-1997, p. 1575, New Orleans, USA.

[44] N.M. Khalil, Heat resistance and thermomechanical behaviour of ultra low and zero cement castables, Br. Ceram. Trans. 103 (1) (2004) 37–41.
[45] K. Jono, J. Mori, Y. Toritani, Effect of alumina grain size on spinel formation, Taikabutsu Overseas 48 (1) (1996) 22–28.
[46] F. Simonin, C. Olagnon, S. Maximilien, G. Fantozzi, Thermomechanical behaviour of high alumina refractory castables with synthetic spinel addition, J. Am. Ceram. Soc. 83 (2000) 2481–2490.
[47] G.E. Goncalves, L.R.M. Bittencourt, The mechanisms of formation of mayenite ($C_{12}A_7$) and the quaternary phase Q(Ca_{20} Al_{26} Mg_3 Si_3 O_{68}) of the system CaO–MgO–Al_2O_3–SiO_2 in magnesia–spinel bricks used in the burning and transition zones of rotary cement kilns, in: Proceedings of UNITECR-2003, pp. 138–141, Osaka.
[48] M. Ramakrishna Rao, Liquidus relations in the quaternary subsystem $CaAl_2O_4$–$CaAl_4O_7$–$Ca_2Al_2SiO_7$–$MgAl_2O_4$, J. Am. Ceram. Soc. 51 (1968) 50–54.
[49] C.A. Schacht (Ed.), Fracture of Refractories; R.C. Bradt, Corrosion of Refractories, Marcel Dekker Inc., New York, 2004, pp. 28–30.
[50] T.K. Gupta, Crack healing in Al_2O_3, MgO and Related Materials, vol. 10, O.J. Wittemore et al. (Ed.), Model of interaction between magnesia with water, Am. Ceram. Soc., Ohio, 1984, pp. 750–766.
[51] D.P.H. Hasselman, Unified theory of thermal shock fracture initiation and crack propagation in brittle ceramics, J. Am. Ceram. Soc. 52 (1969) 600–604.
[52] A.J. Winn, R.I. Todd, Microstructural requirements for alumina–SiC nanocomposites, Br. Ceram. Trans. 98 (5) (1999) 219–224.
[53] S.J. Bennnison, Crack-resistance behaviour in ceramics, in: D.C. Cranmer, D.W. Richerson (Eds.), Mechanical Testing Methodology for Ceramic Design and Reliability, Marcel Dekker Inc, New York, 1998, pp. 43–89 (chapter 3).
[54] C.A. Schacht (Ed.), Refractories Handbook, S. Baxendale, Testing of Refractory Materials, Marcel Dekker Inc., New York, 2004, p. 445.
[55] H.S. Nalwa, Handbook of Nano-Structured Materials and Nanotechnology, 1, Academic Press, USA, 2000, p. 216312, 501 and 534.
[56] R.A. McCauley, Corrsion: a review of some fundamentals, in: G.A. Pecoraro, J.C. Marra, J.T. Wenzel (Eds.), Corrosion of Materials by Molten Glass, Ceramic Transactions, vol. 78, The American Ceramic Society, USA, 1996, pp. 81–89.
[57] C.A. Schacht (Ed.), Refractories Handbook, D.A. Brosnan, Corrosion of Refractories, Marcel Dekker Inc., New York, 2004, p. 43 (chapter 3).
[58] A.R. Cooper, The use of phase diagram in dissolution studies, in: A.M. Alper (Ed.), The Phase Diagrams, Materials Science and Technology, vol. 6, third ed., Academic Press, New York, 1970 (chapter VI).
[59] F.E.Wooley, Prediction of refractory corrosion rate from glass viscosity and composition, in: L.J. Trostel Jr., O.H. Westervill (Eds.), Proceedings of UNITECR-1989, vol.1, pp.768–779.
[60] P. Korgul, P.R. Wilson, W.E. Lee, Microstructural analysis of corroded alumina–spinel castable refractories, J. Eur. Ceram. Soc. 17 (1997) 77–84.
[61] R.K. Sing Raman, Corrosion of nanocrystalline metallic materials, in: Proceedings of International conference on Nanomaterials: Synthesis, Characterisation and Application'', McGrawHill publication, 4–6 November, Kolkata, India, 2004), pp. 154–160.